The Journal of Experimental Biology 216, 4666-4677

doi:10.1242/jeb.093245

RESEARCH ARTICLE

A kinematic model of Kármán gaiting in rainbow trout

Otar Akanyeti and James C. Liao*

The Whitney Laboratory for Marine Bioscience, Department of Biology, University of Florida, 9505 Ocean Shore Boulevard, St Augustine, FL 32136, USA

*Author for correspondence (jliao@whitney.ufl.edu)

SUMMARY

A mechanistic understanding of how fishes swim in unsteady flows is challenging despite its prevalence in nature. Previous kinematic studies of fish Kármán gaiting in a vortex street behind a cylinder only report time-averaged measurements, precluding our ability to formally describe motions on a cycle-by-cycle basis. Here we present the first analytical model that describes the swimming kinematics of Kármán gaiting trout with 70–90% accuracy. We found that body bending kinematics can be modelled with a travelling wave equation, which has also been shown to accurately model free-stream swimming kinematics. However, free-stream swimming and Kármán gaiting are separated in the parameter space; the amplitude, wavelength and frequency values of the traveling wave equation are substantially different for each behavior. During Kármán gaiting, the wave is initiated at the body center, which is 0.2*L* (where *L* is total body length) further down the body compared with the initiation point in free-stream swimming. The wave travels with a constant speed, which is higher than the nominal flow speed just as in free-stream swimming. In addition to undulation, we observed that Kármán gaiting fish also exhibit substantial lateral translations and body rotations, which can constitute up to 75% of the behavior. These motions are periodic and their frequencies also match the vortex shedding frequency. There is an inverse correlation between head angle and body angle: when the body rotates in one direction, the head of the fish turns into the opposite direction. Our kinematic model mathematically describes how fish swim in vortical flows in real time and provides a platform to better understand the effects of flow variations as well as the contribution of muscle activity during corrective motions.

Key words: Kármán gait, kinematic model, kinematics, unsteady flow, vortex street, turbulence.

Received 28 June 2013; Accepted 19 September 2013

INTRODUCTION

Fishes of different body types exhibit similar midline kinematics during steady undulatory locomotion (i.e. free-stream swimming). Common descriptive features of free-stream swimming are: (1) a mechanical wave passes down the body with a speed greater than the swimming speed, (2) the amplitude of the wave increases towards the tail, and (3) the lateral motion of the head is very small at low swimming speeds but increases at higher swimming speeds (Bainbridge, 1963; Gray, 1933; Lauder and Madden, 2006; Marey, 1894; Videler and Wardle, 1978; Wardle et al., 1995; Webb, 1988).

More specifically, these shared characteristics have patterns that can be conveniently quantified. When free-stream swimming kinematics is modeled as a linear combination of sine waves, we see that a single wave is sufficient to describe the motion at every point along the body; the amplitude of higher frequency terms are usually embedded in noise or small compared with the fundamental frequency (Videler and Hess, 1984). Furthermore, the amplitude envelope (i.e. peak-to-peak amplitude of each point along the midline) increases non-linearly towards the tail and the travelling wave propagates with constant speed at the posterior body region (Videler and Hess, 1984).

These findings enable free-stream swimming kinematics to be modeled with a simple travelling wave equation. This equation, with an arbitrary initial phase (ϕ), takes the form:

$$h(x,t) = A(x) \times \sin(kx - \omega t + \phi)\,, \quad (1)$$

where h is the motion perpendicular to flow direction, A is amplitude, k is body wave number, ω is angular frequency, and t and x denote time and position along the body, respectively. The wave initiation point varies with the locomotor mode (thunniform, carangiform, anguilliform), which is defined according to how much of the body participates in the undulatory wave (Breder, 1926). Temporal and spatial periodicity of the equation are determined by the angular frequency ($\omega=2\pi f$, where f is the frequency of undulation) and body wave number ($k=2\pi/\lambda$, where λ is body wavelength), respectively. The speed of the travelling wave (V) is defined by:

$$V = \lambda f\,. \quad (2)$$

The amplitude envelope [$A(x)$] also depends on the locomotor mode. For subcarangiform swimmers such as rainbow trout and mackerel, it is described by a second-order polynomial $A(x)=c_1x+c_2x^2$ (Videler and Hess, 1984), whereas for anguilliform swimmers (e.g. eel) it is approximated by an exponential function (Borazjani and Sotiropoulos, 2009; Tytell and Lauder, 2004).

For free-stream swimming, the travelling wave equation can be integrated with energetic calculations and hydrodynamic models, making it possible to relate fish morphology and kinematics to locomotor propulsion (Cheng and Blickhan, 1994; Cheng et al., 1998; Lighthill, 1971; Lighthill, 1970; Pedley and Hill, 1999; Taylor, 1952; Webb, 1971; Webb, 1975). This would allow an estimation of how much power and thrust is required to swim at a certain speed for a given body shape. From this, we

can evaluate the animal's swimming efficiency (Webb, 1975; Webb, 1988; Webb, 1992).

In natural environments such as rivers and streams, fish commonly encounter unsteady flows, which can fall anywhere along the spectrum of true turbulence to coherent vortex streets. As a result, there is a growing interest in studying how fish swim in unsteady flows (Cotel and Webb, 2012; Cotel et al., 2006; Liao, 2007; Liao and Cotel, 2013; Tritico and Cotel, 2010; Tritico et al., 2007; Webb et al., 2010). However, the kinematic and hydrodynamic models describing swimming in still water or uniform flows are insufficient to describe the locomotion in complex flows. Because of this, our understanding of the effects of unsteady flows on stability, energetics, thrust production and swimming efficiency is greatly compromised.

Examining how fish interact with vortices shed from a cylinder provides a systematic way to study fish–fluid interactions under complex, yet predictable, flow conditions. Additionally, it has been shown that fish save energy when swimming in Kármán vortex streets (i.e. Kármán gait) (Liao et al., 2003a; Liao et al., 2003b; Taguchi and Liao, 2011). A Kármán vortex street is generated behind a cylinder in uniform flow. Flow moving past the cylinder creates vortices that shed alternately from each side of the cylinder. When Reynolds numbers are within 40–100,000, the vortices are staggered regularly as two columnar arrays (Williamson, 1996; Zdravkovich, 1997). This is a powerful setup to swim fish in unsteady flows, as we have the ability to carefully control the flow variables by changing the flow speed and cylinder diameter.

Until now, the term Kármán gait was defined based on (1) the position of the fish in a specific region of the Kármán vortex street and (2) average values of 12 kinematic variables that differed from free-stream swimming (Liao et al., 2003a). However, these average values cannot explain how points along the midline move with respect to each other, and they cannot describe the motions of a fish as it interacts with vortices at each instant in time. This is a limiting factor for biologists, who are interested in analyzing how the whole body interacts with oncoming vortices in real time, and for hydrodynamic modelers and engineers, who seek to evaluate the performance of bio-inspired designs. In this study, we present the first kinematic model that encapsulates midline kinematics of Kármán gaiting in analytical form. Because our model can generate midlines that are very similar to those of live trout, it can be used in the future by biologists to evaluate Kármán gaiting, by roboticists to develop control algorithms that can move bio-inspired robots, and by computational fluid dynamics modelers to simulate fluid–structure interactions.

MATERIALS AND METHODS

Data sets

We developed our model based on extracted midlines from a previous study (Liao et al., 2003a). Briefly, eight rainbow trout [*Onchorhynchus mykiss* (Walbaum 1792); L=10.0±0.3 cm, where L is the total body length] were swum in a flow tank in both free-stream flow and a Kármán vortex street. The flow speed was maintained at $4.5L\ s^{-1}$, and a 5 cm diameter, D-section cylinder was used to generate a vortex street. Vortex shedding frequency and wake wavelength (downstream distance between vortices) were 2.22±0.01 Hz and 20.3±0.1 cm, respectively. The center of mass of each fish was experimentally determined post-mortem for straight-stretched fish by iteratively moving bilateral pins down the body until the antero-posterior pin position for which the body balanced was found. The distance from this point to the tip of the head was then used to determine a fixed point along the body midline of each video frame (Liao et al., 2003a). Here, we call this point the body center (BC), which refers to the center of mass in previous work (Liao et al., 2003a; Liao et al., 2003b; Liao, 2004; Taguchi and Liao, 2011).

In this study, we were interested in analyzing the fish motion perpendicular to the nominal flow direction. We therefore subtracted the downstream–upstream translation from the original midlines to overlap all midlines. The experimental data were analyzed with customized scripts in MATLAB (vR2009b, The MathWorks, Natick, MA, USA).

Modelling free-stream swimming kinematics

Fish midlines in free-stream swimming were used as a reference to evaluate the performance of the Kármán gait model. We modeled free-stream swimming kinematics using the traveling wave equation presented in Eqn 1, with the wave starting at the base of the cranium ($x=l-0.2L$, where $l=0.2L$ to $1.0L$). The amplitude envelope was modelled with a second-order polynomial $A(x)=c_1x+c_2x^2$. The parameters of the travelling wave equation (c_1, c_2, λ and f) were estimated empirically based on the original midlines. Amplitude coefficients c_1 and c_2 were calculated from the amplitude envelope using least square methods. The tail beat frequency was computed as an average number of tail beat cycles in 1 s.

Wave speed was estimated by tracking wave crests along the body over a given time period. After modelling the midline of each frame with a third-order polynomial, a wave crest was identified as a local minimum or maximum point using first and second derivative tests. The wave speed was estimated by averaging the slope of these crest trajectories. Once tail beat frequency and wave speed were known, the body wavelength was computed using Eqn 2.

Fourier analysis on Kármán gait kinematics

In order to guide our modeling approach for Kármán gait kinematics, it was crucial to first determine whether undulation plays a role during Kármán gaiting. This required establishing the existence of an undulatory wave passing down the body. Videler and Hess (Videler and Hess, 1984) previously advanced an efficient method based on Fourier series analysis to quantify such waves during free-stream swimming. In this method, the lateral motion of each point along the midline was represented by a periodic cosine function. The parameters of the cosine function (amplitude, frequency and phase) were estimated using least square algorithms to minimize the error between the actual and predicted motions in time. Given that all points along the midline oscillated with the same frequency, it was possible to analyze how the values of amplitude and phase in every cosine function changed along the body. A linear phase-position relationship indicated the presence of a travelling wave in the anterior–posterior direction with a constant speed. As a counter example, a constant phase-position relationship would suggest that all points along the body reached to maximum amplitude at the same time, which is a characteristic of standing waves or motions of a rigid body.

In this study, we adopted a similar approach to analyze Kármán gait midlines using the fast-Fourier transform (FFT). In particular, we computed the FFT of the lateral motion for each point along the midline. We determined whether the lateral motion of all midline points could be represented by the same fundamental frequency. The existence of such a frequency would enable us to analyze the changes in amplitude and phase as a function of position along the body. In addition, a linear phase-position relationship would show that a travelling wave was also present during Kármán gaiting. If this was the case, it would be important to know where the wave

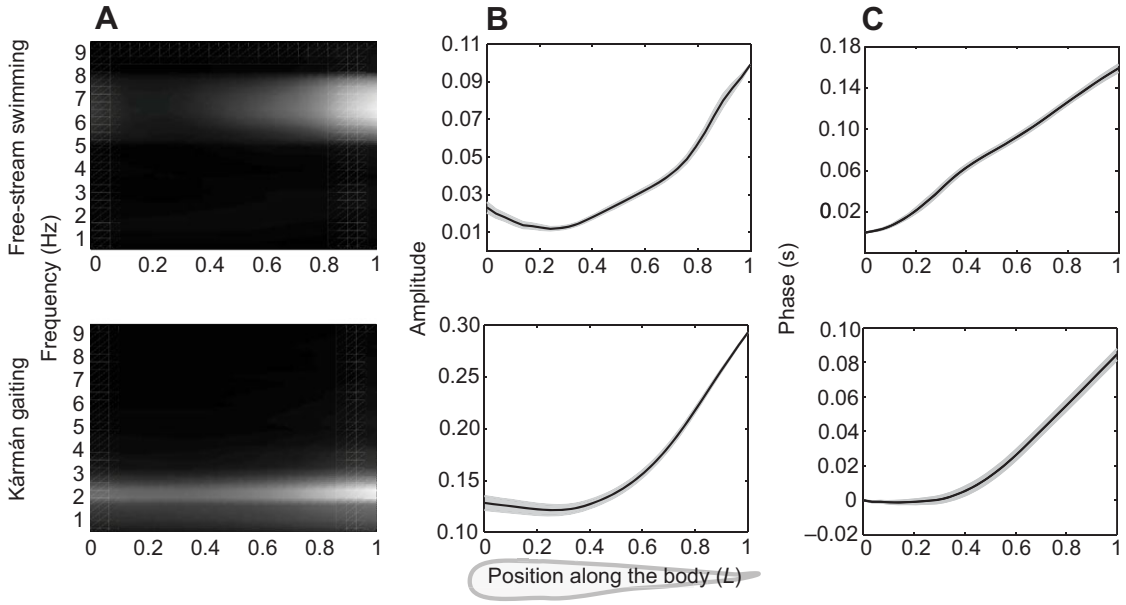

Fig. 1. Fourier analysis (normal bin distribution, bin size 0.1 Hz) of fish midline kinematics during free-stream swimming and Kármán gaiting at 4.5*L* s^{-1}. (A) Normalized frequency spectrum where black (white) denotes the frequency with the smallest (largest) lateral amplitude. Both free-stream swimming and Kármán gaiting exhibited periodic lateral oscillations, where the dominant frequency was 6.6±0.1 and 2.2±0.05 Hz, respectively. (B) Mean amplitude curves (solid line) at dominant frequency (grey shaded area shows ±s.e.m.). In both behaviors, the amplitude of lateral oscillations was smallest at the mid-body region and increased gradually towards the tail. During Kármán gaiting, body amplitudes at all locations were larger than during free-stream swimming. (C) Mean phase curves (solid line) at dominant frequency (gray shaded area shows ±s.e.m.). A traveling wave was evident for both behaviors. In Kármán gaiting, the wave started at the body center (0.4*L*), which was ~0.2*L* posterior to the starting point of free-stream swimming fish. In both behaviors, the wave speed was constant along the posterior body (~60 cm s^{-1} for free-stream swimming and ~75 cm s^{-1} for Kármán gaiting fish). The free-stream swimming amplitude and phase curves of trout are very similar to those of saithe and mackerel (Videler and Hess, 1984).

started (i.e. the position at which the phase started increasing linearly) and how the amplitude of the wave changed along the body. We applied FFT analysis to the midlines from free-stream swimming to highlight the differences between free-stream swimming and Kármán gaiting. Note that our FFT analysis on free-stream swimming trout revealed results very similar to those presented previously (Videler and Hess, 1984).

The FFT analysis, as shown in Fig. 1, revealed three major biological findings: (1) during Kármán gaiting, all points along the body oscillated with the same frequency, confirming our hypothesis that the midline kinematics could be described with one dominant frequency (Fig. 1A); (2) the amplitude of this frequency was smallest at a body position 0.3*L* from the snout (0*L*) and increased quadratically towards the tail (Fig. 1B); and (3) the phase was relatively constant at the anterior body (0*L* to 0.4*L*) and increased linearly in the posterior body (after 0.4*L*). This suggested that the body wave was initiated at the body center (0.4*L*) and travelled posteriorly at a constant speed (Fig. 1C). Thus, FFT analysis confirmed that Kármán gaiting fish possess a travelling wave down the body just as in free-stream swimming.

Modeling Kármán gait kinematics

We next proceeded with developing the model based on the travelling wave equation. We observed a major difference between Kármán gaiting and free-stream swimming, which was the presence of lateral translation and rotation in addition to undulation (Fig. 2A). The amount of lateral translation and body rotation due to recoil movements of free-stream swimming fish was negligible compared with the magnitudes of motion measured in Kármán gaiting.

In classical mechanics, whole-body translation and rotation is collectively known as rigid body motions. We hypothesize that Kármán gaiting can be modeled as a superimposition of midlines that come from undulation, rigid body motions and head motion. We test our hypothesis with a modeling approach that can be summarized in three steps. (1) We apply linear transformation to Kármán gait midlines in order to separate head and undulatory motion from rigid body motions (Fig. 2C). After linear transformation, we obtain four sets of midlines accounting for undulation, head motion, lateral translation and body rotation (Fig. 2D). (2) We model each set of midlines with a separate equation and estimate their parameters empirically. We then obtain the full Kármán gait model by summing the four sets of midlines. (3) We evaluate the full model by comparing its midlines with the actual midlines of the fish.

Step 1. Decomposing Kármán gaiting midlines into four fundamental motion components: lateral translation, body rotation, head motion and body bending

To extract rigid body motions, a body region that remained straight during Kármán gaiting needed to be identified. We found that the section between the base of the cranium and the body center satisfied this criterion (0.2*L* to 0.4*L*; Fig. 2B). Our FFT analysis suggested that the midline points in this region were oscillating with a constant phase and a similar amplitude (Fig. 1B,C). This indicates that the midline points in this region were moving together without bending. For each midline, we fitted a straight line (i.e. rigid body line) to represent this section of the midline using the polyfit function in MATLAB. The rotation of the body was estimated as the angle (θ_{body}) between the rigid body line and the axis of flow. To isolate head motion and body bending, the raw midlines were rotated automatically using a rotation matrix to set the body angle to zero. The center of rotation (Fig. 2B, black circle) was chosen as the

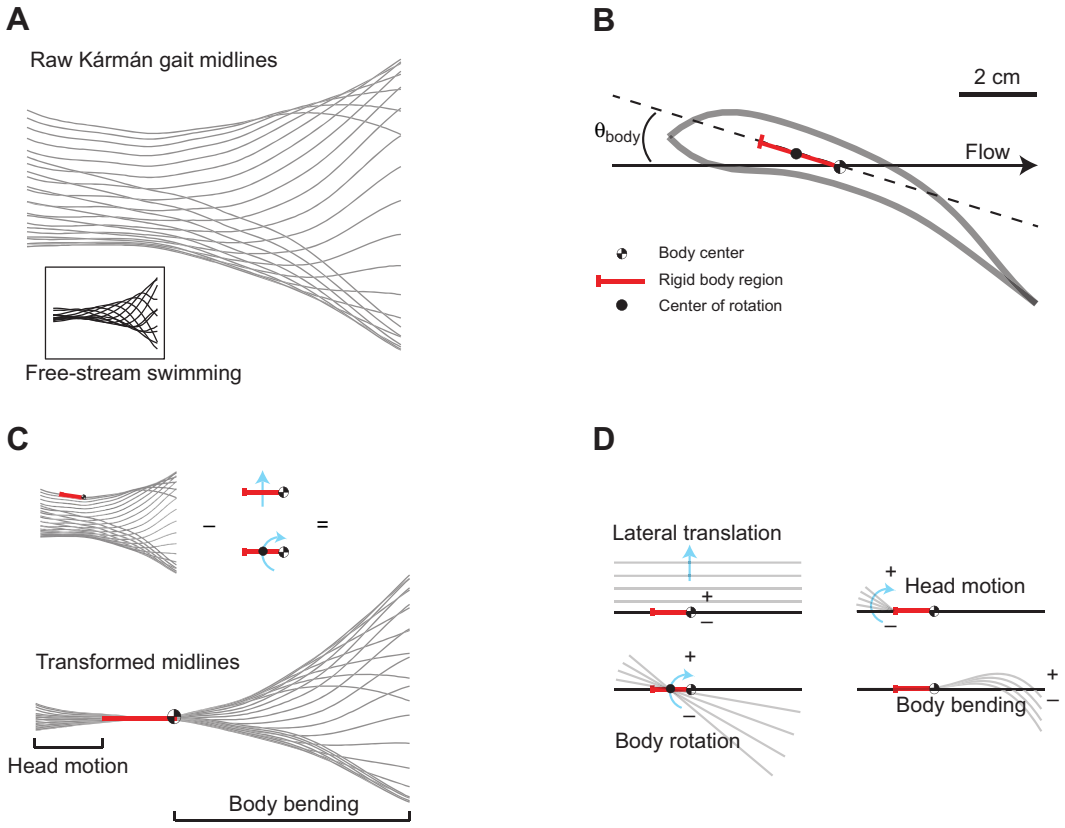

Fig. 2. (A) Original fish midlines recorded during Kármán gaiting and free-stream swimming. (B) During Kármán gaiting, the body region between the cranium and the body center was straight (red line). This allowed us to distinguish lateral translation and rotation (rigid body motions) from undulatory motion. We estimated the rotation of the body as an angle (θ_{body}) between the axis of the rigid body region and the axis of flow. (C) Transformed midlines, after removing body rotation and lateral translation, revealed head motion and bending of the posterior body (between the body center and tail). (D) Overall, Kármán gait kinematics can be largely explained by four fundamental motion components: lateral translation, body rotation, head motion and body bending.

midpoint of the rigid body lines ($0.3L$). This point also corresponded to the minimum amplitude point along the body (Fig. 1B). We then subtracted the lateral translation, which was estimated as the motion of the rigid body line perpendicular to the flow direction.

After lateral translation and body rotation were subtracted from the raw midlines, the transformed midlines consisted of head motion and body bending (Fig. 2C). The body amplitudes at the rigid body region were minimal, suggesting that our midline transformation was appropriate. To minimize the numerical noise, we smoothed these midlines using a low-pass filter with a 10 Hz cut-off frequency.

In conclusion, we decomposed Kármán gait kinematics into four fundamental motion components: lateral translation, body rotation, body bending and head motion (Fig. 2D). During lateral translation and rotation, all points along the midline translated and rotated with the same magnitude. The head motion was defined as the head angle with respect to flow axis, with the assumption that the cranium ($0L$ to $0.2L$) was rigid. Body bending only included the region that was posterior to the body center (i.e. posterior midline).

Step 2. Modeling each motion component individually and obtaining the full Kármán gait model

We independently modeled each of the four motion components of Kármán gaiting [body bending ($h_{bending}$), lateral translation ($h_{translation}$), body rotation ($h_{rotation}$) and head motion (h_{head}), where h refers to motion perpendicular to flow direction], and ultimately obtained our full model by combining these motions. We modelled body bending kinematics using the traveling wave equation presented in Eqn 1, where the wave started at the body center, $x=l-0.4L$, where $l=0.4L$ to $1.0L$. For simplicity we assume that the distance between the most anterior point and the body center was constant ($0.4L$), which in reality changed by 2%. The amplitude was described by $A(x)=c_1x+c_2x^2$ and the parameters of the travelling wave equation (c_1, c_2, λ and f) were estimated empirically just like in free-stream swimming.

We modeled lateral displacement ($d_{translation}$), body angle ($\theta_{rotation}$) and head angle (θ_{head}) as a periodic function:

$$d_{translation}(t) = A_{translation}\sin(2\pi f_{translation}t + \phi_{translation}), \quad (3)$$

$$\theta_{rotation}(t) = A_{rotation}\sin(2\pi f_{rotation}t + \phi_{rotation}), \quad (4)$$

$$\theta_{head}(t) = A_{head}\sin(2\pi f_{head}t + \phi_{head}). \quad (5)$$

We estimated the parameters of the sine wave (amplitude, frequency and phase with respect to body bending) using least square methods to minimize the error between actual and predicted motions. Because $d_{translation}$, $\theta_{rotation}$ and θ_{head} were single values for a given t, we entered them into Eqns 6 to 8 to generate midlines accounting for lateral translation ($h_{translation}$), body rotation ($h_{rotation}$) and head motion (h_{head}), respectively.

$$h_{translation}(x,t) = d_{translation}(t), (x = l, \text{ where } l = 0L \text{ to } 1.0L), \quad (6)$$

$$h_{rotation}(x,t) = x \times \sin[\theta_{rotation}(t)], \quad (x = l - 0.3L, \text{ where } l = 0L \text{ to } 1.0L), \quad (7)$$

$$h_{head}(x,t) = x \times \sin[\theta_{head}(t)], \quad (x = l - 0.2L, \text{ where } l = 0L \text{ to } 0.2L). \quad (8)$$

The overall model was obtained by combining the four motion components:

$$h_{kg} = h_{translation} + h_{rotation} + h_{head} + h_{bending}. \quad (9)$$

Step 3. Evaluation of the model

We evaluated the performance of the overall model (h_{kg}) by comparing the midline points of the fish (h_{fish}) and the model (h_{model})

frame by frame. The percentage amplitude difference $D(x,t)$ was computed using the following equation:

$$D(x,t) = \left[h_{\text{fish}}(x,t) - h_{\text{model}}(x,t) / h_{\text{fish}}^{\max}(x) \right], \qquad (10)$$

where $0<x<L$ and $0<t<T$ (T is the duration of a video sequence). $h_{\text{fish}}^{\max}(x)$ was the maximum absolute value of $h_{\text{fish}}(x,t)$ for each x. If the model was a good fit, the two midlines should overlay each other for each frame [i.e. $D(x,t)$ approached 0] and $D(x,t)$ should be distributed randomly across time and space. Any identifiable pattern would reveal a systematic error and indicate that not all fish motions could be captured by the model. We computed minimum, maximum and mean absolute difference (MAD) to summarize $D(x,t)$. We assumed the model was acceptable if the MAD was less than 25%. Given that our model does not take into account muscle activity or variations in the flow, MAD is not expected to reach zero. For each x, we computed the mean absolute value of $D(x,t)$ to analyze how $D(x,t)$ varies as a function of anterior–posterior position. For each t, we computed the linear correlation coefficient between actual and modeled midlines to measure their similarity.

Statistical analysis: relationships between lateral acceleration, tail beat amplitude, and head and body angle

We further investigated the inter-relationships between the four motion components; in particular, we examined lateral acceleration *versus* tail beat amplitude and head angle, and head angle *versus* body angle and tail beat amplitude. To identify these relationships, we used a linear regression analysis ($P<0.05$). When a phase offset between two kinematic variables was detected, the cross-correlation coefficient was computed to estimate the time offset.

RESULTS

Model and its evaluation

All values are presented as means ± s.e.m. Table 1 presents the estimated parameters for Eqn 1 (h_{bending}) and Eqns 6 to 8 ($h_{\text{translation}}$, h_{rotation} and h_{head}). We obtained the full kinematic model (h_{kg}) by superimposing the midlines of h_{bending}, $h_{\text{translation}}$, h_{rotation} and h_{head} according to Eqn 9.

The midline kinematics of the model were in good agreement with the kinematics of live fish, where both modeled and actual midlines were statistically indistinguishable (i.e. kinematic variables such as amplitude envelope, tail beat frequency, body wavelength, maximum head angle and maximum curvature measured from both actual and modeled midlines had the same value) (Fig. 3).

We further evaluated the performance of the full kinematic model by comparing the actual and modeled midlines frame by frame over several tail beat cycles for one representative fish. We found that the model was fairly good at approximating the motions of the fish. A residual color map [$D(x,t)$] shows a comprehensive temporal picture of the percentage amplitude difference between the fish and the model at all points along the body (Fig. 4A). The minimum and maximum percentage amplitude difference was ±0.60% and the MAD was 23.73±4.31%.

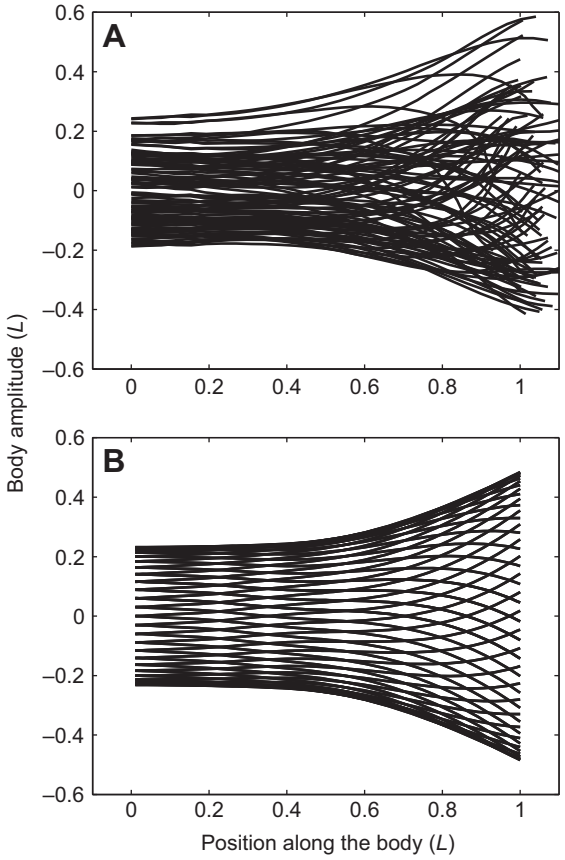

Fig. 3. Comparison of actual and modelled midlines. (A) Raw midlines obtained from a trout Kármán gaiting for six tail beat cycles. (B) Midlines generated by the kinematic model. Although small corrective motions could not be captured by the model, in general the main components of Kármán gaiting, such as the amplitude envelope and curvature, were recovered.

Fig. 4B shows examples of live fish (blue) and modeled (red) midlines at three time points [$D(x,t)$=~0, model directly overlapped fish; $D(x,t)>0$, model was ahead of the fish; and $D(x,t)<0$, model was behind the fish]. In all three situations the shape of the midlines for both model and fish was similar. Furthermore, the comparison of the model to fish at six locations along the body did not reveal any significant pattern in amplitude difference (Fig. 4C).

We quantified the similarity between fish and model midlines by computing a linear correlation coefficient for each time frame. High correlation coefficients (>0.9, except for a few frames) indicated very good match between the fish and model midlines (Fig. 5A). The mean correlation coefficient was 0.81±0.05.

Table 1. Estimated parameter values of the Kármán gait model for a rainbow trout swimming in a vortex street at 4.5L s^{-1} behind a 5 cm diameter cylinder

	h_{bending} (L)	$h_{\text{translation}}$ (L)	h_{rotation} (L)	h_{head} (L)
A	c_1=0.01±0.02L c_2=0.51±0.10L	0.24±0.05L	7.75±1.0 deg	3.80±0.22 deg
f (Hz)	2.20±0.10	2.10±0.10	2.10±0.10	2.10±0.10
λ (L)	2.80±0.20	–	–	–
ϕ (deg)	0	0	–72.19±5.40	107.71±8.10

The Kármán gait model was a superimposition of four motion components: body bending (h_{bending}; Eqn 1), lateral translation ($h_{\text{translation}}$; Eqns 3 and 6), body rotation (h_{rotation}; Eqns 4 and 7) and head motion (h_{head}; Eqns 5 and 8). A, amplitude; f, frequency; λ, wavelength; ϕ, phase.

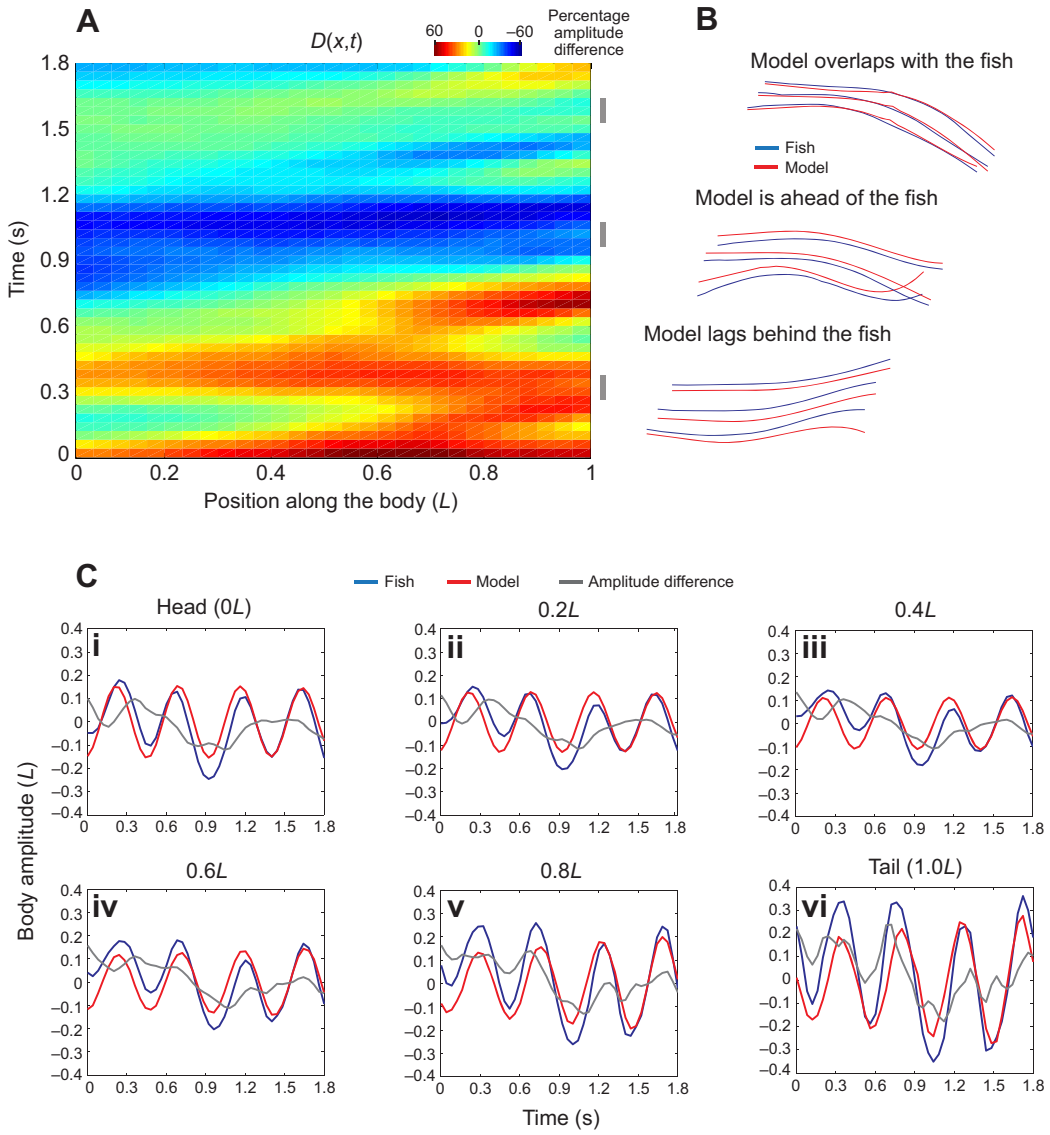

Fig. 4. Evaluation of the full kinematic model on one representative fish during several tail beat cycles. (A) A residual color map showing the percentage amplitude difference [$D(x,t)$] between the fish and model midlines across time and position along the body. (B) Series of fish (blue) and model (red) midlines at three selected time points (gray bars in A). (C) Comparison between fish and model motion at six locations along the body (i–vi) show that there is no systematic error between the model and the fish.

Fig. 5B shows the mean absolute value of $D(x,t)$ as a function of x, which was relatively smaller at the anterior body and increased slightly towards the tail. A mean absolute value less than 30% verifies that the model performed well in predicting fish midlines. A comprehensive analysis across multiple fish (N=6) revealed similar results; the minimum and maximum percentage amplitude difference was within ±0.75% and the MAD was 22.20±5.89%. The mean correlation coefficient was 0.77±0.13 (N=6).

Contribution of each motion component to Kármán gaiting

Our analysis shows that the midline kinematics of Kármán gaiting fish can be represented as a superimposition of four midlines generated by four motion components. Isolating each of the four motion components enabled us to evaluate their individual contributions to Kármán gaiting kinematics. We calculated the area swept out by the amplitude envelope of each motion and compared it with the area of original Kármán gait midlines. We found that the contribution of each motion component was not evenly distributed. Lateral translation comprised the majority of the kinematics (~67.8%), followed by body bending (~19.9%), body rotation (~9.0%) and head motion (~3.4%; N=6).

In a similar manner, we had the opportunity to evaluate the performance of the individual models (h_{bending}, $h_{\text{translation}}$, h_{rotation} and h_{head}) in terms of a percentage of $D(x,t)$. Our individual model evaluation showed that $D(x,t)$ came mainly from the difference in lateral translation (~70.0%), followed by body bending (~18.6%), body rotation (~7.5%) and head motion (~3.9%; N=6). The model assumed that the lateral translation of fish had constant amplitude. During the actual experiments, we observed that the amplitude depended on the dynamics of the vortex street, which often varied in time. Therefore, amplitude offsets between the fish and model were expected, whereas differences in midline shapes would indicate that the model performed poorly.

Relationship between lateral acceleration and tail beat amplitude

Our kinematic model assumed that the four motion components were independent from each other, and thus interactions between these components were not considered. However, we recognize that these motions might be interconnected and influence each other. For instance, we noticed that some of the fish motions that could not be predicted by the model could be explained by the lateral acceleration of the fish. We observed a high correlation between

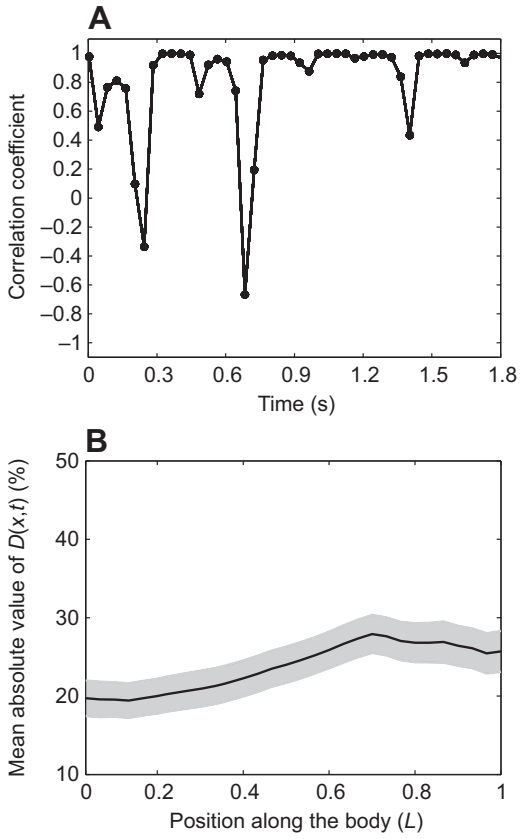

Fig. 5. Evaluation of the full kinematic model as a function of time and position along the body. (A) Correlation coefficient showing the similarity in shape between fish and model midlines for each frame. (B) Mean absolute value of percentage amplitude difference [$D(x,t)$] as a function of position along the body (x) (the standard error is shown in gray).

lateral acceleration and tail beat amplitude. Tail beat amplitude lagged behind lateral acceleration by ~90 deg (Fig. 6A, P<0.05, N=6). The data in the phase-space plot between the tail beat amplitude and lateral acceleration were distributed as a two-dimensional toroid (Fig. 6B). This toroid pattern is indicative of the fact that the tail beat amplitude mimics the lateral acceleration, but with a time delay. When lateral acceleration was higher, the tail beat amplitude was also higher. Likewise, when fish were accelerating faster, the tail was also moving faster.

Relationship between head angle, body angle and lateral acceleration

When we analyzed the relationship between head and body angle, we saw that head angle decreased linearly with body angle according to y=–0.48x (r^2=0.44, P<0.05, N=6; Fig. 7A). When body angle was at one extreme, the head angle was at the opposite extreme. Head angle also decreased with lateral acceleration according to y=–0.34x (r^2=0.55, P<0.05, N=6; Fig. 7B). Head angle was at a maximum when the fish was changing its direction of motion, which corresponds to a time of maximum lateral acceleration.

Comparison between free-stream swimming and Kármán gaiting

We looked at the differences between the midline kinematics of body bending during Kármán gaiting and free-stream swimming. The performance of the Kármán gait model was compared with the performance of the free-stream, travelling wave model. We considered the Kármán gait model successful if it had performed at least as well as the free-stream swimming model.

Kinematic models describing Kármán gaiting and free-stream swimming kinematics (only body bending) are presented in Table 2. Body bending of both free-stream swimming and Kármán gaiting was described accurately by the travelling wave equation. There was no statistical difference in the performance of the two models. When we compared the parameters of the two travelling wave equations, Kármán gaiting fish had larger body amplitudes and body wavelength than free-stream swimming fish. In Kármán gaiting fish, the tail beat frequency, which matched the vortex shedding frequency, was significantly lower than that found for free-stream swimming.

The relationship between head angle and tail beat amplitude was also distinct between free-stream swimming and Kármán gaiting fish. During free-stream swimming, the head angle increased linearly with the tail beat amplitude according to y=0.70x (r^2=0.56, P<0.05, N=6; Fig. 8A). When the tail beat amplitude was at its furthest lateral excursion, the head angle was also maximally at that side. In contrast, during Kármán gaiting there was a phase offset between the head angle and tail beat amplitude. The tail beat amplitude lagged behind the head angle by ~72 deg (P<0.05, N=6; Fig. 8B).

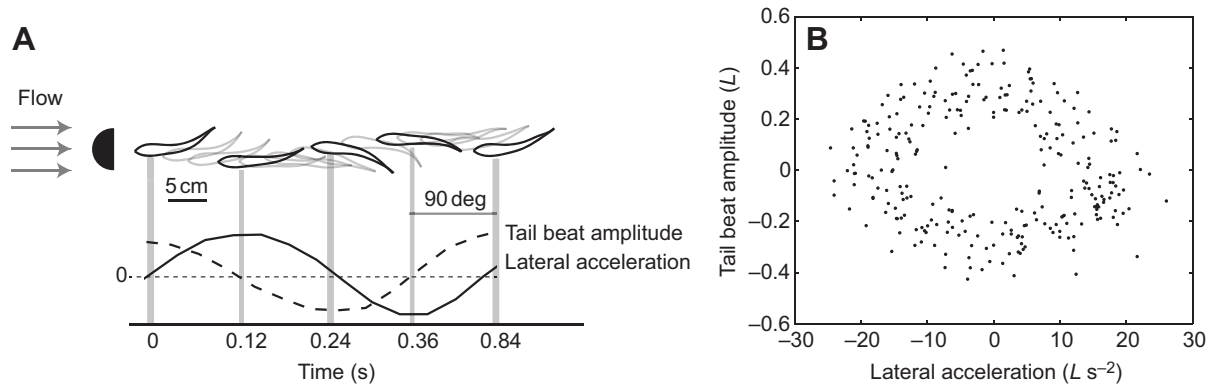

Fig. 6. Relationship between lateral acceleration (solid line) and tail beat amplitude (dashed line) of Kármán gaiting trout. (A) Lateral acceleration and tail beat amplitude profiles of one representative fish during one tail beat cycle. Tail beat amplitude lagged behind lateral acceleration by ~90 deg. When the anterior body was in the middle of the vortex street (t=0 s, t=0.24 s and t=48 s, thick lines), the tail beat amplitude was at its most lateral excursion. At these time points, the lateral acceleration was zero (horizontal dashed line). In contrast, lateral acceleration was at a maximum when the anterior body changed direction of motion (t=0.12 s and t=0.36 s, thin lines). In these instances, the tail beat amplitude was at the middle of the vortex street and continued moving along the same direction. (B) Phase-space plot between tail beat amplitude and lateral acceleration confirms the correlation between these two variables.

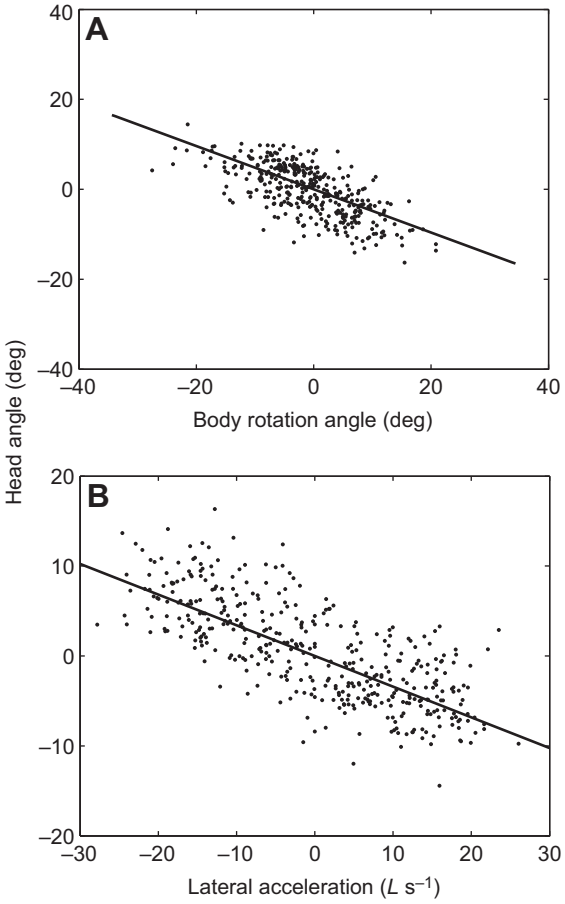

Fig. 7. (A) Relationship between body rotation angle and head angle of Kármán gaiting fish. Head angle decreased linearly with body angle (y=–0.48x, r^2=0.44, P<0.05, N=8). (B) Relationship between lateral acceleration and head angle of Kármán gaiting fish. Head angle also decreased linearly with lateral acceleration (y=–0.34x, r^2=0.55, P<0.05, N=8).

DISCUSSION

Generalization of the Kármán gait model

We present a quantitative model that is able to accurately predict the midline kinematics of rainbow trout (L=10 cm) swimming in the vortex street generated behind a 5 cm cylinder in a flow speed of 4.5L s^{-1}. Because our model was developed under a specific experimental condition, we acknowledge that as physical parameters (fish length, cylinder diameter and flow velocity) change, so will the values of our model. Exploring this parameter space is not trivial, but past work has already linked some of these parameters to wake variables (Akanyeti and Liao, 2013; Liao et al., 2003a). We used these studies to develop a scalable model that incorporates cylinder diameter and flow speed. In other words, we can rewrite the parameters of our model (Eqn 9) as a function of cylinder diameter and flow speed.

We start with the travelling wave equation (Eqn 1). At intermediate flow speeds (30 cm s^{-1}<U<80 cm s^{-1}), frequency of the undulation (f) matched the vortex shedding frequency (f_{vs}) (Akanyeti and Liao, 2013; Liao et al., 2003a), which is described by:

$$f = f_{vs} = \frac{StU}{D}, \tag{11}$$

where D is the cylinder diameter, U is the flow speed and St is the Strouhal number. St is approximately 0.2 for D-shaped cylinders (Zdravkovich, 1997). Body wavelength (λ) was 25% larger than the wake wavelength (λ_{wake}) (Akanyeti and Liao, 2013; Liao et al., 2003a),

$$\lambda = \frac{1.25\lambda_{wake}}{L}, \tag{12}$$

and wake wavelength is only dictated by the cylinder diameter ($\lambda_{wake}=D/St$). In smaller fish (10 cm), body wavelength is 1.4 times longer than the body wavelength given in Eqn 12 (Akanyeti and Liao, 2013). Peak-to-peak tail beat amplitude was around D/L for the two cylinder conditions tested previously (Liao et al., 2003a). This suggests that the amplitude envelope of undulation can be initially approximated according to:

$$A(x) = \frac{Dx^2}{L}, \tag{13}$$

where we assume that c_1~0, given that c_1<<c_2. The phase relationship between drifting vortices and body center was 180 deg (Liao et al., 2003b). We use this phase relationship:

$$\phi = \pi, \tag{14}$$

to synchronize the midlines generated by the model with the Kármán vortex street. Finally, these relationships (Eqns 11 to 14) are incorporated into Eqn 1 to generalize the body bending during Kármán gaiting:

$$h_{bending} = \frac{Dx^2}{L}\sin\left[2\pi\left(\frac{StLx}{1.25D} - \frac{StU}{D}t\right) + \pi\right]. \tag{15}$$

The amplitude of the lateral motion ($d_{translation}$) depends on the cylinder diameter according to $A_{translation}$=0.5D/L (Akanyeti and Liao, 2013). So Eqn 3 can be rewritten as:

$$d_{translation} = \frac{0.5D}{L}\sin\left(2\pi\frac{StU}{D}t\right), \tag{16}$$

Table 2. Kinematic comparison of body bending between free-stream swimming and Kármán gaiting at 4.5L s^{-1}

	Free-stream swimming	Kármán gaiting
Wave initiation point (L)	0.20	0.40
Average wave speed (L s^{-1})	1.20	1.60
$A(x)$ (L)	0.10x^2+0.02x	0.50x^2+0.04x
λ (L)	1.0±0.30	2.80±0.20
f (Hz)	6.60±0.40	2.20±0.10
Min./max. percentage amplitude difference (%)	±18	±17
Mean percentage amplitude difference (%)	10.50±4.2	12.24±3.1
Phase angle between head angle and tail beat amplitude (deg)	0	72.0

Body bending of free-stream swimming and Kármán gaiting fish can be accurately modeled with the traveling wave equation (Eqn 1). However, estimated parameters are distinct for each behavior.

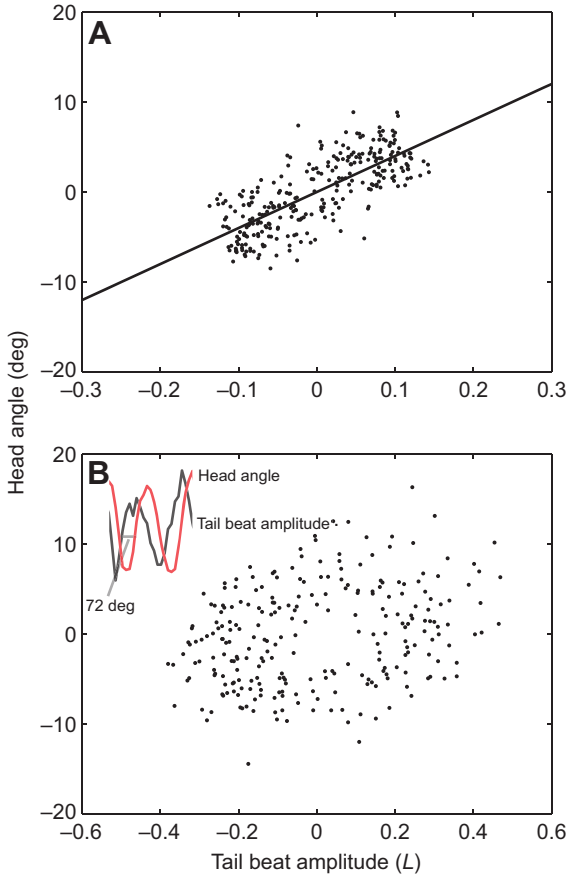

Fig. 8. Relationship between tail beat amplitude and head angle. (A) In free-stream swimming, head angle increased linearly with tail beat amplitude (y=0.70x, r^2=0.56, P<0.05, N=8). This indicates that when the tail beat amplitude was at one extreme, the head angle was also maximally at that side (i.e. in phase). (B) In contrast, during Kármán gaiting the tail beat amplitude lagged behind head angle by ~72 deg (r^2=0.70, P<0.05, N=8).

and entered into Eqn 6 to generate lateral translation midlines. While we concentrated on the motion components that had the largest effects on Kármán gaiting, the comparatively minor components such as amplitudes of head angle and body angle and their phase relationship with respect to Eqn 15 remain to be explored as a function of physical parameters. Because the contributions of body rotation and head motion are relatively small (<15%) compared with body bending and lateral motion, Eqns 15 and 16 allow us to systematically predict a substantial portion of the Kármán gait midline kinematics for a given set of flow speed and cylinder diameter conditions (Fig. 9).

Overall, our kinematic model represents an important step forward in the study of locomotion in unsteady flows by defining the Kármán gait analytically with a formalized equation. Thus, kinematic variables taken from future empirical studies can be entered into our model to generate the whole-body movements matching the Kármán gait kinematics with 70–90% accuracy.

Kármán gaiting is undulatory swimming superimposed with translational and rotational motion

During Kármán gaiting, undulatory motion is modulated by lateral translation and body rotation, which constitute up to 75% of the behavior. Given that fishes cannot translate or rotate as a rigid body in still water, the rigid body motions observed during Kármán gaiting must be involuntary and induced by the hydrodynamic forces present in the vortex streets. For a fish holding station in a Kármán vortex street, the staggered arrangement of vortices creates an oscillating pressure gradient across the left and right side of the body. This pressure gradient determines the direction and strength of the force. Fish exploit these lateral forces to maintain a certain distance downstream from the cylinder (Beal et al., 2006; Liao, 2004).

During Kármán gaiting, the body wave is initiated at the body center, which is approximately 0.2L posterior to the initiation point of free-stream swimming. Fourier analysis on the motions of a dead trout towed behind a cylinder shows that in a completely passive body, the wave starts at the base of the cranium, similar to free-stream swimming (Fig. 10). This suggests that the change in the location of the wave initiation point during Kármán gaiting is not due to the passive fish–fluid interactions. We postulate that live Kármán gaiting fish strategically activate their anterior muscles in order to adopt a straight posture in the mid-body region; as a result this arrangement changes the location of the initiation point. We believe that the interaction between fish and fluid in the mid-body region is more critical than the posterior region. Thus, instead of drifting vortices, a point source directed at the mid-body region would be sufficient to generate swimming kinematics similar to Kármán gaiting. If our postulation is correct, fish may keep the mid-body region from bending in order to provide a local axial control surface to harness the appropriate fluid forces.

Our results show that a simple travelling wave can describe both free-stream swimming and Kármán gaiting kinematics. However, whether the travelling wave is generated actively through muscular activity or passively due to flow-induced motions varies depending on the flow regime. In freestream swimming, an antero-posterior wave of red muscle activity drives the propagation of the wave (Jayne and Lauder, 1995a). In contrast, during Kármán gaiting the lateral motion of fish dictates its substantial body bending. The undulatory waves seem to be generated passively as a result of the acceleration while the fish is being buffeted from side to side by the fluid (Liao et al., 2003b). Several findings support this argument. First, muscle recordings indicate that Kármán gaiting fish activate only the anterior red axial muscles (Liao, 2004). Second, dead trout temporarily generate a mechanical wave similar to live fish (Beal et al., 2006). Third, in this study we observe a high correlation between the lateral acceleration and tail beat amplitude of the fish.

In free-stream swimming, the traveling wave runs along the posterior body with constant speed (Jayne and Lauder, 1995b). Similarly, in Kármán gaiting the wave speed is largely constant along the posterior body and it is higher than the flow speed. The mechanisms leading to constant body wave speed may vary between free-stream swimming and Kármán gaiting. In free-stream swimming, sequential muscle activation keeps the body wave speed constant. In Kármán gaiting, drifting vortices may keep the body wave speed constant. The question of how critical it is for wave speed to be constant during both free-stream swimming and Kármán gaiting remains to be addressed.

Fish balance of body rotation with the head movements

In free-stream swimming, head motions are coupled with body undulations. Lighthill (Lighthill, 1993) suggested that fish control the angular velocity of the head by periodic muscle activations in order to compensate for sideslip accelerations. This would minimize pressure difference across the head and in turn would reduce hydrodynamic drag during swimming.

In contrast, we knew very little about the role of the head during Kármán gaiting prior to this study. Our results show that there is a

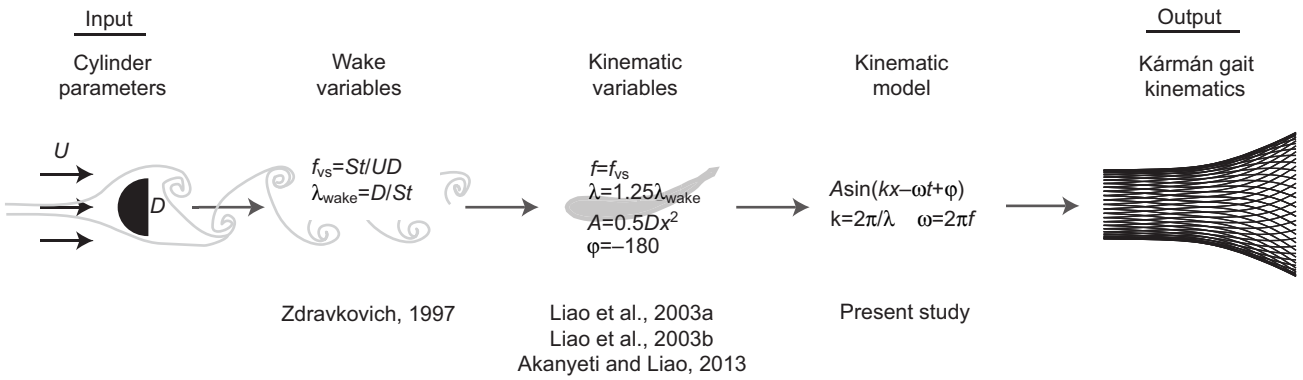

Fig. 9. Flow diagram describing the relationship between cylinder parameters and body bending kinematics of the Kármán gait. *D*, cylinder diameter; *f*, tail beat frequency; f_{vs}, vortex shedding frequency; *St*, Strouhal number; *U*, flow speed; λ_{wake}, wake wavelength; λ, body wavelength; φ, phase difference between body center and a drifting vortex.

high inverse correlation between head angle and body angle. We hypothesize that fish counterbalance the body rotation using their head for stability. When the body rotates, the head moves in the opposite direction to keep the fish aligned upstream and prevent extreme body angles. Experiments have shown that even a rigid foil positioned in a vortex street can generate thrust (Beal et al., 2006). If passive lift generation plays a major role in Kármán gaiting, an excess amount of body rotation may cause the fish to drift downstream. At large body angles, fish may not generate enough lift because of increased flow separation. However, we emphasize that this argument is inherited from aerodynamic studies on two-dimensional rigid foils and may be less applicable to three-dimensional fish swimming in vortex streets.

Cycle-by-cycle analysis of fish–fluid interactions

As expected, actual fish motions are more complex than the predictions of a model that does not account for internal (muscle) and external (vortices) forces. Our model rests on the assumption that fish swim in an ideal vortex street with turbulent features (i.e. vortex size, strength, spacing and frequency) that do not vary in time. In reality, there is a certain amount of unpredictable variation in the behavior of vortex streets, which would influence the kinematics of the fish. In this sense, our model represents theoretical Kármán gait kinematics in ideal hydrodynamic conditions and can be used as a norm to highlight instantaneous fish motions that are novel.

For example, a cycle-by-cycle comparison between the tail beat amplitude of the fish and the predicted values from the model for a selected swimming sequence is shown in Fig. 11A. The model (red) provides an average tail beat motion by which to evaluate the actual motions of the fish (blue). At times, fish moved as the model predicted (Fig. 11B, red directly overlapping blue) but at other times it did not. Over the course of experiments, we have identified several patterns that deviated from the model (Fig. 11C–F).

These patterns may provide hypotheses of when muscle or fin activity is recruited during Kármán gaiting. Simultaneous flow visualization, muscle recordings and kinematics would allow us to test some of these hypotheses. Our long-term goal is to develop hydrodynamic models that incorporate fluid forces, muscle activity and biomechanical properties of the fish to identify the underlying mechanisms of Kármán gait kinematics.

Lessons for roboticists

In addition to quantifying the Kármán gait, our model provides insights that can guide the contributions of embodiment and control strategy as a resource for future robotics work. Given that the majority of the body waves during Kármán gaiting are likely generated passively, we hypothesize that it is more important for a

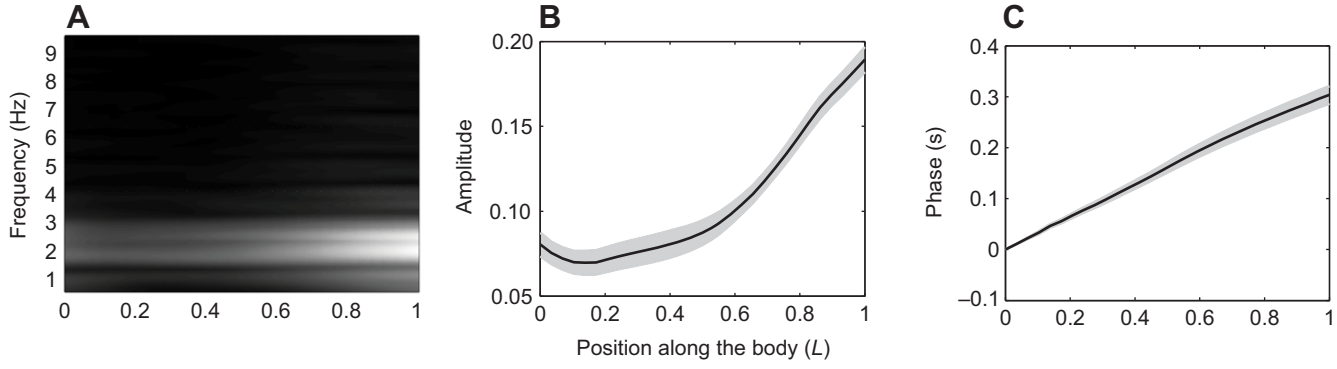

Fig. 10. Fourier analysis of the midline kinematics of a dead trout while in the vortex street [*L*=17.8 cm, flow speed=57 cm s^{-1}, cylinder diameter=5 cm (Beal et al., 2006)]. (A) Normalized frequency spectrum revealed that the dominant frequency is 2.20±0.10 Hz, similar to a live Kármán gaiting trout (Fig. 1A). (B) Mean amplitude curve (solid line) across six tail beat cycles (gray shaded area shows ±s.e.m.) indicated that body amplitudes of dead trout were smaller than those of live trout (Fig. 1B). (C) Increasing phase lag from head to tail in the mean phase curve (solid line, gray shaded area shows ±s.e.m.) indicated that the traveling wave along the body was initiated more anteriorly than in a live trout (Fig. 1C). This suggests that live fish actively control the anterior body to prevent wave formation.

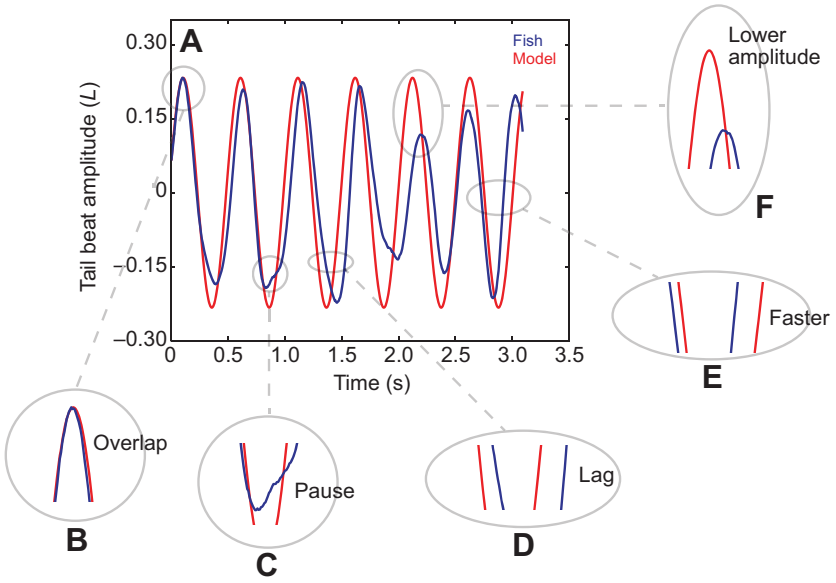

Fig. 11. (A) Cycle-by-cycle comparison of tail beat amplitude between a fish (red) and the model (blue) for a selected seven tail beat sequences. At times, the fish moved as the model predicted (B, red directly overlapping blue), but not at other times. Several time points show examples of a deviation from the model. (C) Fish interrupted a continuous sweep with a pause. (D) Within a cycle, the fish lagged increasingly behind the model. (E) Fish moved faster than the model predicts. (F) Tail beat amplitude was lower than that of the model.

robot to control its head and the anterior body than its posterior body. If hydrodynamic forces are harnessed appropriately at the anterior body, a travelling wave is generated passively at the posterior body starting from the body center. This represents a paradigm shift in the field of autonomous robotics locomotion, which traditionally emphasizes the control of the posterior body (Alvarado, 2007; Liu and Hue, 2006; Salumäe and Kruusmaa, 2013; Stefanini et al., 2012). Our results suggest that head control is crucial for steering and improving stability by counterbalancing body rotations and lateral translation.

In theory, building a Kármán gaiting robot by actively controlling the tail beat frequency to match the vortex shedding frequency may seem like a reasonable strategy. However, we believe that visco-elastic properties of the body alone are likely to produce Kármán gaiting for short periods. In this way, the control functionality is outsourced to properties of the embodiment itself.

This study provides a formal definition of Kármán gaiting kinematics that, as in free-stream swimming, recognizes the central role of axial-body undulation. This advances our understanding of fish locomotion by showing that fish can navigate extremely different hydrodynamic environments based on the same general pattern of body undulation.

LIST OF SYMBOLS AND ABBREVIATIONS

A	amplitude
A_{head}	amplitude of head motion
$A_{rotation}$	amplitude of body rotation
$A_{translation}$	amplitude of lateral motion
c_1	first coefficient of second-degree polynomial
c_2	second coefficient of second-degree polynomial
D	cylinder diameter
$D(x,t)$	percentage amplitude difference
$d_{translation}$	lateral displacement
f	frequency of undulation
f_{head}	frequency of head motion
$f_{rotation}$	frequency of body rotation
$f_{translation}$	frequency of lateral motion
f_{vs}	vortex shedding frequency
h	motion perpendicular to flow direction
$h_{bending}$	model midlines (undulatory motion)
h_{fish}	fish midlines
h_{head}	model midlines (head motion)
h_{kg}	model midlines (full)
$h_{rotation}$	model midlines (body rotation)
$h_{translation}$	model midlines (lateral translation)
k	body wave number
L	body length
MAD	mean absolute value of percentage amplitude difference
N	number of fish
St	Strouhal number
t	time
T	video sequence duration
U	flow speed
V	body wave speed
x	position along the body
θ_{head}	head angle
$\theta_{rotation}$	body rotation angle
λ	body wavelength
λ_{wake}	wake wavelength
ϕ	phase
ϕ_{head}	phase of head motion
$\phi_{rotation}$	phase of body rotation
$\phi_{translation}$	phase of lateral motion
ω	angular frequency

ACKNOWLEDGEMENTS

We would like to thank Elaine C. Seaver, Melanie Haehnel, Rafael Levi and two anonymous reviewers for comments leading to the improvement of the manuscript. We also thank George V. Lauder for the generous use of his equipment.

AUTHOR CONTRIBUTIONS

J.C.L. designed and performed the experiments. O.A. analyzed the data. J.C.L. and O.A. contributed to data interpretation, prepared the figures and wrote the manuscript.

COMPETING INTERESTS

No competing interests declared.

FUNDING

Support was provided by the National Institutes of Health (NIH 1RO1DC010809-01) and the National Science Foundation (NSF IOS-1257150) to J.C.L. Deposited in PMC for release after 12 months.

REFERENCES

Akanyeti, O. and Liao, J. C. (2013). The effect of flow speed and body size on Karman gait kinematics in rainbow trout. *J. Exp. Biol.* **216**, 3442-3449.

Alvarado, P. V. (2007). *Design of Biomimetic Compliant Devices for Locomotion in Liquid Environments*. PhD dissertation, Massachusetts Institute of Technology, Cambridge, MA, USA.

Bainbridge, R. (1963). Caudal fin and body movements in the propulsion of some fish. *J. Exp. Biol.* **40**, 23-56.
Beal, D. N., Hover, F. S., Triantafyllou, M. S., Liao, J. C. and Lauder, G. V. (2006). Passive propulsion in vortex wakes. *J. Fluid Mech.* **549**, 385-402.
Borazjani, I. and Sotiropoulos, F. (2009). Numerical investigation of the hydrodynamics of anguilliform swimming in the transitional and inertial flow regimes. *J. Exp. Biol.* **212**, 576-592.
Breder, C. M. (1926). The locomotion of fishes. *Zool. N. Y.* **4**, 159-256.
Cheng, J. Y. and Blickhan, R. (1994). Bending moment distribution along swimming fish. *J. Theor. Biol.* **167**, 337-348.
Cheng, J. Y., Pedley, T. J. and Altringham, J. D. (1998). Continuous dynamic beam model for swimming fish. *Philos. Trans. R. Soc. B.* **353**, 981-997.
Cotel, A. J. and Webb, P. W. (2012). The challenge of understanding and quantifying fish responses to turbulence-dominated physical environments. In *Natural Locomotion in Fluids and on Surfaces: Swimming, Flying, and Sliding* (ed. S. Childress, A. Hosoi, W. W. Schultz and Z. J. Wang), pp. 15-34. Heidelberg: Springer.
Cotel, A. J., Webb, P. W. and Tritico, H. (2006). Do brown trout choose locations with reduced turbulence? *Trans. Am. Fish. Soc.* **135**, 610-619.
Gray, J. (1933). Studies in animal locomotion. I. The movement of fish with special reference to the eel. *J. Exp. Biol.* **10**, 88-104.
Jayne, B. C. and Lauder, G. V. (1995a). Red muscle motor patterns during steady swimming in largemouth bass: effects of speed and correlations with axial kinematics. *J. Exp. Biol.* **198**, 1575-1587.
Jayne, B. C. and Lauder, G. V. (1995b). Speed effects on midline kinematics during steady undulatory swimming of largemouth bass, *Micropterus salmoides*. *J. Exp. Biol.* **198**, 585-602.
Lauder, G. V. and Madden, P. G. A. (2006). Learning from fish: kinematics and hydrodynamics for roboticists. *Int. J. Autom. Comput.* **4**, 325-335.
Liao, J. C. (2004). Neuromuscular control of trout swimming in a vortex street: implications for energy economy during the Karman gait. *J. Exp. Biol.* **207**, 3495-3506.
Liao, J. C. (2007). A review of fish swimming mechanics and behaviour in altered flows. *Philos. Trans. R. Soc. B* **362**, 1973-1993.
Liao, J. C. and Cotel, A. (2013). Effects of turbulence on fish swimming in aquaculture. In *Swimming Physiology of Fish: Towards Using Exercise to Farm A Fit Fish in Sustainable Aquaculture* (ed. A. P. Palstra and J. V. Planas), pp. 109-127. Berlin: Springer.
Liao, J. C., Beal, D. N., Lauder, G. V. and Triantafyllou, M. S. (2003a). The Kármán gait: novel body kinematics of rainbow trout swimming in a vortex street. *J. Exp. Biol.* **206**, 1059-1073.
Liao, J. C., Beal, D. N., Lauder, G. V. and Triantafyllou, M. S. (2003b). Fish exploiting vortices decrease muscle activity. *Science* **302**, 1566-1569.
Lighthill, M. J. (1970). Aquatic animal propulsion of high hydromechanical efficiency. *J. Fluid Mech.* **44**, 265-301.
Lighthill, J. (1971). Large-amplitude elongated body theory of fish locomotion. *Proc. R. Soc. B* **179**, 125-138.
Lighthill, J. (1993). Estimates of pressure differences across the head of a swimming clupeid fish. *Philos. Trans. R. Soc. B* **341**, 129-140.
Liu, J. and Hue, H. (2006). Biologically inspired behaviour design for autonomous robotic fish. *Int. J. Autom. Comput.* **4**, 336-347.
Marey, E. J. (1894). *Le Mouvement.* Paris: Masson.
Pedley, T. J. and Hill, S. J. (1999). Large-amplitude undulatory fish swimming: fluid mechanics coupled to internal mechanics. *J. Exp. Biol.* **202**, 3431-3438.
Salumäe, T. and Kruusmaa, M. (2013). Flow-relative control of an underwater robot. *Proc. R. Soc. A* **469**, 20120671.
Stefanini, C., Orofino, S., Manfredi, L., Mintchev, S., Marrazza, S., Assaf, T., Capantini, L., Sinibaldi, E., Grillner, S., Wallén, P. et al. (2012). A novel autonomous, bioinspired swimming robot developed by neuroscientists and bioengineers. *Bioinspir. Biomim.* **7**, 025001.
Taguchi, M. and Liao, J. C. (2011). Rainbow trout consume less oxygen in turbulence: the energetics of swimming behaviors at different speeds. *J. Exp. Biol.* **214**, 1428-1436.
Taylor, G. (1952**).** Analysis of the swimming of long and narrow animals. *Proc. R. Soc. A* **214**, 158-183.
Tritico, H. M. and Cotel, A. J. (2010). The effects of turbulent eddies on the stability and critical swimming speed of creek chub (*Semotilus atromaculatus*). *J. Exp. Biol.* **213**, 2284-2293.
Tritico, H. M., Cotel, A. J. and Clarke, J. N. (2007). Development, testing and demonstration of a portable submersible miniature particle imaging velocimetry device. *Meas. Sci. Technol.* **18**, 2555-2562.
Tytell, E. D. and Lauder, G. V. (2004). The hydrodynamics of eel swimming: I. Wake structure. *J. Exp. Biol.* **207**, 1825-1841.
Videler, J. J. and Hess, F. (1984). Fast continuous swimming of two pelagic predators, saithe (*Pollachius virens*) and mackerel (*Scomber scombrus*): a kinematic analysis. *J. Exp. Biol.* **109**, 209-228.
Videler, J. J. and Wardle, C. S. (1978). New kinematic data from high speed cine film recordings of swimming cod (*Gadus morhua*). *Neth. J. Zool.* **28**, 465-484.
Wardle, C. S., Videler, J. J. and Altringham, J. D. (1995). Tuning in to fish swimming waves: body form, swimming mode and muscle function. *J. Exp. Biol.* **198**, 1629-1636.
Webb, P. W. (1971). The swimming energetics of trout. I. Thrust and power output at cruising speeds. *J. Exp. Biol.* **55**, 489-520.
Webb, P. W. (1975). Hydrodynamics and energetics of fish propulsion. *Bull. Fish. Res. Bd. Canada* **190**, 1-159.
Webb, P. W. (1988). 'Steady' swimming kinematics of tiger musky, an esociform accelerator, and rainbow trout, a generalist cruiser. *J. Exp. Biol.* **138**, 51-69.
Webb, P. W. (1992). Is the high cost of body/caudal fin undulatory swimming due to increased friction drag or inertial recoil? *J. Exp. Biol.* **162**, 157-166.
Webb, P. W., Cotel, A. J. and Meadows, L. M. (2010). Waves and eddies: effects on fish behavior and habitat distribution. In *Fish Locomotion, an Eco-ethological Perspective* (ed. P. Domenici and B. G. Kapoor), pp. 1-39. Enfield, NH: Science Publishers.
Williamson, C. H. K. (1996). Vortex dynamics in the cylinder wake. *Annu. Rev. Fluid Mech.* **28**, 477-539.
Zdravkovich, M. M. (1997). *Flow Around Circular Cylinders: A Comprehensive Guide Through Flow Phenomena, Experiments, Applications, Mathematical Models, and Computer Simulations.* Oxford: Oxford University Press.